



Ultra-compact tunable silicon nanobeam cavity with an energy-efficient graphene micro-heater

ZHENZHEN XU,¹ CIYUAN QIU,^{1,*} YUXING YANG,¹ QINGMING ZHU,¹
XINGHONG JIANG,¹ YONG ZHANG,¹ WEILU GAO,² AND YIKAI SU^{1,3}

¹State Key Lab of Advanced Optical Communication Systems and Networks, Department of Electronic Engineering, Shanghai Jiao Tong University, Shanghai 200240, China

²Department of Electrical and Computer Engineering, Rice University, Houston, Texas 77005, USA

³yikaisu@sjtu.edu.cn

*qiuciyuan@sjtu.edu.cn

Abstract: We propose and experimentally demonstrate an ultra-compact silicon photonic crystal nanobeam (PCN) cavity with an energy-efficient graphene micro-heater. Owing to the PCN cavity with an ultra-small optical mode volume of $0.145 \mu\text{m}^3$, the light-matter interaction is greatly enhanced and the thermo-optic (TO) tuning efficiency is increased. The TO tuning efficiency is measured to be as high as 1.5 nm/mW , which can be further increased to 3.75 nm/mW based on numerical simulations with an optimized structure. The time constants with a rise time constant of $\tau_{\text{rise}} = 1.11 \mu\text{s}$ and a fall time constant of $\tau_{\text{fall}} = 1.47 \mu\text{s}$ are obtained in the experiment.

© 2017 Optical Society of America

OCIS codes: (130.3120) Integrated optics devices; (160.5298) Photonic crystals; (160.4236) Nanomaterials; (230.5750) Resonators.

References and links

1. M. Asghari and A. V. Krishnamoorthy, "Silicon photonics: energy-efficient communication," *Nat. Photonics* **5**(5), 268–270 (2011).
2. D. X. Xu, A. Densmore, P. Waldron, J. Lapointe, E. Post, A. Del age, S. Janz, P. Cheben, J. H. Schmid, and B. Lamontagne, "High bandwidth SOI photonic wire ring resonators using MMI couplers," *Opt. Express* **15**(6), 3149–3155 (2007).
3. M. Casalino, M. Iodice, L. Sirleto, I. Rendina, and G. Coppola, "Asymmetric MSM sub-bandgap all-silicon photodetector with low dark current," *Opt. Express* **21**(23), 28072–28082 (2013).
4. Q. Xu, B. Schmidt, S. Pradhan, and M. Lipson, "Micrometre-scale silicon electro-optic modulator," *Nature* **435**(7040), 325–327 (2005).
5. V. R. Almeida, C. A. Barrios, R. R. Panepucci, M. Lipson, M. A. Foster, D. G. Ouzounov, and A. L. Gaeta, "All-optical switching on a silicon chip," *Opt. Lett.* **29**(24), 2867–2869 (2004).
6. R. L. Espinola, M. C. Tsai, J. T. Yardley, and R. M. Osgood, "Fast and low-power thermo-optic switch on thin silicon-on-insulator," *IEEE Photonics Technol. Lett.* **15**(10), 1366–1368 (2003).
7. P. Dong, W. Qian, H. Liang, R. Shafiqi, D. Feng, G. Li, J. E. Cunningham, A. V. Krishnamoorthy, and M. Asghari, "Thermally tunable silicon racetrack resonators with ultralow tuning power," *Opt. Express* **18**(19), 20298–20304 (2010).
8. M. R. Watts, W. A. Zortman, D. C. Trotter, G. N. Nielson, D. L. Luck, and R. W. Young, "Adiabatic resonant microrings (ARMs) with directly integrated thermal microphotonics," in *Conference on Lasers and Electro-Optics* (Optical Society of America, 2009), paper CPDB10.
9. K. S. Novoselov, A. K. Geim, S. V. Morozov, D. Jiang, Y. Zhang, S. V. Dubonos, I. V. Grigorieva, and A. A. Firsov, "Electric field effect in atomically thin carbon films," *Science* **306**(5696), 666–669 (2004).
10. A. K. Geim and K. S. Novoselov, "The rise of graphene," *Nat. Mater.* **6**(3), 183–191 (2007).
11. X. Du, I. Skachko, A. Barker, and E. Y. Andrei, "Approaching ballistic transport in suspended graphene," *Nat. Nanotechnol.* **3**(8), 491–495 (2008).
12. F. Wang, Y. Zhang, C. Tian, C. Girit, A. Zettl, M. Crommie, and Y. R. Shen, "Gate-variable optical transitions in graphene," *Science* **320**(5873), 206–209 (2008).
13. M. Liu, X. Yin, E. Ulin-Avila, B. Geng, T. Zentgraf, L. Ju, F. Wang, and X. Zhang, "A graphene-based broadband optical modulator," *Nature* **474**(7349), 64–67 (2011).
14. X. T. Gan, R. J. Shiue, Y. D. Gao, I. Meric, T. F. Heinz, K. Shepard, J. Hone, S. Assefa, and D. Englund, "Chip-integrated ultrafast graphene photodetector with high responsivity," *Nat. Photonics* **7**(11), 883–887 (2013).

15. Y. Wang, Y. Shao, D. W. Matson, J. Li, and Y. Lin, "Nitrogen-doped graphene and its application in electrochemical biosensing," *ACS Nano* **4**(4), 1790–1798 (2010).
16. A. A. Balandin, S. Ghosh, W. Bao, I. Calizo, D. Teweldebrhan, F. Miao, and C. N. Lau, "Superior thermal conductivity of single-layer graphene," *Nano Lett.* **8**(3), 902–907 (2008).
17. J. Liu, I. Watanabe, K. Yoshida, and M. Atsuta, "Joint strength of laser-welded titanium," *Dent. Mater.* **18**(2), 143–148 (2002).
18. S. Gan, C. Cheng, Y. Zhan, B. Huang, X. Gan, S. Li, S. Lin, X. Li, J. Zhao, H. Chen, and Q. Bao, "A highly efficient thermo-optic microring modulator assisted by graphene," *Nanoscale* **7**(47), 20249–20255 (2015).
19. D. Schall, M. Mohsin, A. A. Sagade, M. Otto, B. Chmielak, S. Suckow, A. L. Giesecke, D. Neumaier, and H. Kurz, "Infrared transparent graphene heater for silicon photonic integrated circuits," *Opt. Express* **24**(8), 7871–7878 (2016).
20. L. H. Yu, Y. L. Yin, Y. C. Shi, D. X. Dai, and S. L. He, "Thermally tunable silicon photonic microdisk resonator with transparent graphene nanoheaters," *Optica* **3**(2), 159–166 (2016).
21. S. Yan, X. Zhu, L. H. Frandsen, S. Xiao, N. A. Mortensen, J. Dong, and Y. Ding, "Slow-light-enhanced energy efficiency for graphene microheaters on silicon photonic crystal waveguides," *Nat. Commun.* **8**, 14411 (2017).
22. S. M. Song, J. K. Park, O. J. Sul, and B. J. Cho, "Determination of work function of graphene under a metal electrode and its role in contact resistance," *Nano Lett.* **12**(8), 3887–3892 (2012).
23. C. T. Derose, M. R. Watts, R. W. Young, D. C. Trotter, G. N. Nielson, W. A. Zortman, and R. D. Kekatpure, "Low power and broadband 2×2 silicon thermo-optic switch," in *Conference on Optical Networking and Communication* (Optical Society of America, 2012), paper OThM3.
24. P. Dong, W. Qian, H. Liang, R. Shafiqi, N. N. Feng, D. Feng, X. Zheng, A. V. Krishnamoorthy, and M. Asghari, "Low power and compact reconfigurable multiplexing devices based on silicon microring resonators," *Opt. Express* **18**(10), 9852–9858 (2010).
25. C. Qiu, T. Pan, W. Gao, R. Liu, Y. Su, and R. Soref, "Proposed high-speed micron-scale spatial light valve based on a silicon-graphene hybrid structure," *Opt. Lett.* **40**(19), 4480–4483 (2015).
26. T. Y. Gu, N. Petrone, J. F. Mcmillan, A. V. D. Zande, M. B. Yu, G. Q. Lo, D. L. Kwong, J. Hone, and C. W. Wong, "Regenerative oscillation and four-wave mixing in graphene optoelectronics," *Nat. Photonics* **6**(8), 554–559 (2012).
27. Y. G. Zhang and Y. C. Shi, "Ultra-low power consumption tunable photonic crystal nanobeam cavity based on suspended ridge waveguides," in *Conference on Nanoelectronics* (IEEE, 2016), paper 7589347.

1. Introduction

Silicon photonics is considered as an ideal platform for on-chip integration, owing to the advantages of compact footprint, low power consumption, and compatibility with complementary metal-oxide-semiconductor (CMOS) processes [1]. To date, various integrated optical devices based on silicon photonics have been demonstrated, such as optical filters [2], photodetectors [3], electro-optical modulators [4], and electro-optical switches [5]. By incorporating these silicon photonic devices, versatile and reconfigurable photonic networks can be realized. In these photonic networks, thermal tuning is often applied with metal heaters, commonly made of Titanium, on top of the silicon waveguides by using the relatively high thermo-optic (TO) coefficient of silicon ($\sim 1.84 \times 10^{-4}/\text{K}$) [6]. To avoid the metal absorption, a thick SiO_2 layer is usually introduced between the silicon layer and the metal heater layer. Since the SiO_2 layer has a poor heat conductivity, it reduces the heating efficiency and slows down the tuning speed. In order to enhance the heating efficiency, free-standing silicon racetrack resonators and waveguides of different doping levels have been demonstrated with high tuning efficiencies [7,8]. However, mechanical instability, slow heating speed, and complicated fabrication processes are issues that remain to be solved.

Graphene, a single sheet of carbon atoms in a hexagonal lattice, has generated tremendous interests due to its attractive properties [9,10], such as high carrier mobility of $\sim 200,000 \text{ cm}^2\text{v}^{-1}\text{s}^{-1}$ at room temperature [11], ultra-broad absorption bandwidth, and tunable Fermi level [12]. Thus, graphene has been incorporated to implement novel optoelectronic devices such as ultrafast optical modulators [13], ultra-broadband photodetectors [14], and ultra-sensitive optical sensors [15]. Specifically, monolayer graphene has a low optical absorption of $\sim 2.3\%$ for vertically incident light [13], so it can directly contact with the silicon waveguides. Graphene also has a high thermal conductivity of up to $5,300 \text{ W/m} \cdot \text{K}$ [16], which is ~ 300 times higher than that of Titanium [17]. With these unique properties, graphene is considered as an excellent material for transparent micro-heaters integrated on optical devices.

Some silicon photonic devices with graphene micro-heaters have been reported, including silicon micro-ring resonators [18,19] and micro-disc resonators [20]. However, the TO tuning efficiencies of these devices were limited due to the insufficient light-matter interactions. Recently, a high-efficiency graphene micro-heater on a slow-light silicon photonic crystal waveguide was demonstrated [21]. With the help of the slow-light effect, the TO tuning efficiency of this device was increased to 1.07 nm/mW. Based on these reported results, one can find that the tuning efficiency can be increased by enhancing the light-matter interaction, which can be achieved through shrinking the mode volume of the device. If the mode volume is decreased, the heated volume, needing to cover the mode volume for the effective TO tuning, is also reduced and thus the heating efficiency is increased.

In this paper, we propose and demonstrate a silicon photonic crystal nanobeam (PCN) cavity with an energy-efficient graphene micro-heater. Since the PCN cavity can achieve an ultra-small mode volume of $0.145 \mu\text{m}^3$, the light-matter interaction is highly enhanced. The tuning efficiency is as high as 1.5 nm/mW, which can be potentially increased to 3.75 nm/mW based on simulations with an optimized structure. The tuning efficiency in the experiment is primarily limited by the heating power loss at the graphene sheet for electrical connections. The time constants with a rise time constant of $\tau_{\text{rise}} = 1.11 \mu\text{s}$ and a fall time constant of $\tau_{\text{fall}} = 1.47 \mu\text{s}$ are obtained.

2. Device structure

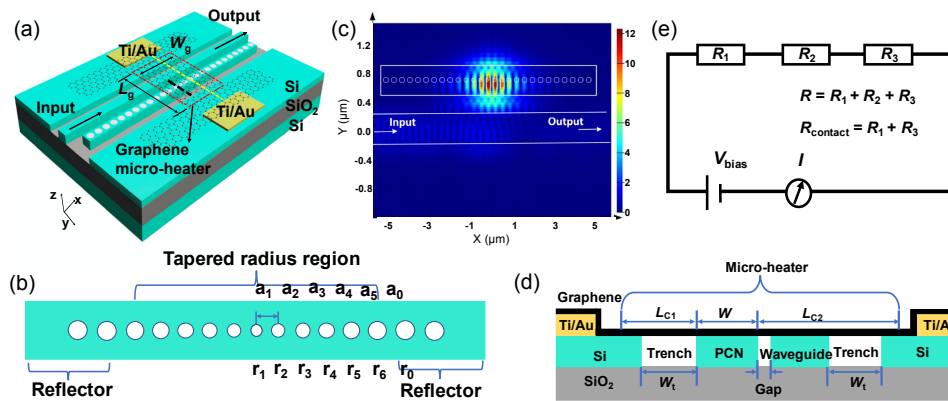


Fig. 1. (a) Three-dimensional schematic illustration of the device based on a silicon PCN cavity structure and a graphene micro-heater. The graphene micro-heater is shown by the red dashed lines. (b) Schematic showing the PCN cavity which is symmetric with respect to its center, where r_i ($i = 0, 1, 2, 3, 4, 5, 6$) is the radius of the hole and a_i is the distance between the two holes. (c) Simulated electric field distribution of the PCN cavity structure at the resonance wavelength. (d) The cross-section of the proposed device corresponding to the yellow dashed line in (a). Here the graphene micro-heater is suspended over the trenches whose widths (W_i) are both set to $1 \mu\text{m}$. (e) Equivalent circuit of the device.

The structure of the device is shown in Fig. 1(a), which includes a silicon PCN cavity side-coupled to a bus waveguide with a graphene sheet on top. The nanobeam waveguide etched with an array of air-holes forms a Fabry-Perot (F-P) cavity, consisting of a central-taper section and two side-reflector sections. The taper section with 11 holes is designed to reduce scattering loss and avoid the phase mismatch between the photonic crystal fundamental Bloch mode and the waveguide mode. The reflectors with 18 holes serve as two symmetrical mirrors to guarantee that the light is highly reflected within the communication band. As shown in Fig. 1(b), the reflector sections with $a_0 = 405 \text{ nm}$ and $r_0 = 113 \text{ nm}$ are tapered down along six holes symmetrically around the center to $a_1 = 309 \text{ nm}$ and $r_1 = 86 \text{ nm}$. The gap between the PCN waveguide and the bus waveguide is 70 nm . Based on these parameters, a finite-difference-time-domain (FDTD) simulation is performed to obtain the electric field

distribution of the PCN cavity at the resonance wavelength. As shown in Fig. 1(c), the light power is tightly concentrated in a volume of $0.145 \mu\text{m}^3$ and the effective length for the thermal tuning is only $\sim 1.8 \mu\text{m}$. The graphene micro-heater is placed on top of the PCN cavity while the length and the width of the graphene micro-heater are denoted as L_g and W_g , respectively. As shown in the cross-sectional diagram of the device [Fig. 1(d)], the graphene micro-heater has three parts with lengths of L_{c1} , w , and L_{c2} , respectively. Here w denotes the length of graphene on top of the nanobeam cavity which is the same as the width of the nanobeam waveguide of $\sim 0.5 \mu\text{m}$. L_{c1} and L_{c2} are the lengths of the graphene for the electrical connections. Note that, the graphene micro-heater is suspended over the trenches and can be easily broken in the fabrication processes if $L_{c1} < 2 \mu\text{m}$ or $L_{c2} < 2.5 \mu\text{m}$. Since L_{c1} and L_{c2} should be as short as possible to reduce the extra heating power loss in the electrical connections, $L_{c1} = 2 \mu\text{m}$ and $L_{c2} = 2.5 \mu\text{m}$ are chosen in the experiments. Thus, the length of the graphene micro-heater (L_g) can be calculated as $L_g = w + L_{c1} + L_{c2} = 5 \mu\text{m}$. As the heated volume needs to cover the mode volume of the PCN cavity, the width of the graphene micro-heater (W_g) should be wider than $1.8 \mu\text{m}$. Furthermore, W_g has a strong effect on the extinction ratio (ER) of the transmission spectrum due to the graphene absorption. In order to obtain good optical performances, W_g is set to $1.8 \mu\text{m}$. The equivalent circuit of the proposed structure is depicted in Fig. 1(e). The total resistance (R) includes two parts, i.e., the resistance of the two Au electrode/graphene contacts ($R_1 + R_3$) and the resistance of the graphene micro-heater (R_2).

3. Device fabrication and measured results

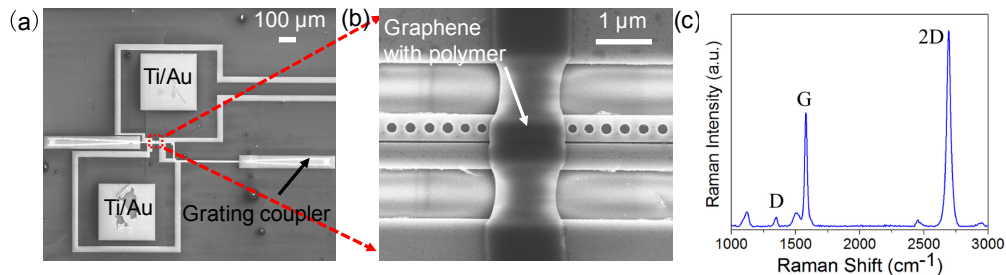


Fig. 2. (a) SEM image of the device. (b) Zoom-in view for the nanobeam waveguide with the graphene micro-heater on top. (c) Raman spectrum of transferred graphene.

The device was fabricated on a silicon-on-insulator (SOI) wafer with a 220-nm-thick top silicon layer. The PCN cavity was defined by the processes of electron beam lithography (EBL) and inductive coupling plasma (ICP) etching. Then 10 nm/100 nm Ti/Au electrodes on the silicon layer were deposited through EBL and lift-off processes. Monolayer graphene grown by chemical vapor deposition (CVD) was wet-transferred on top of the whole SOI wafer. The graphene layer was patterned by EBL and oxygen plasma etching processes. The scanning electron microscope (SEM) image of the device is shown in Fig. 2(a). The zoom-in view of the PCN cavity with the graphene micro-heater is provided in Fig. 2(b). Here the polymethyl methacrylate (PMMA) used for graphene patterning was not removed to prevent the graphene from damage. The low thermal conductivity ($\sim 0.19 \text{ W/m} \cdot \text{K}$) of the PMMA would not introduce obvious influence on the thermal behaviors of the device [20]. The measured Raman spectrum of the transferred graphene is presented in Fig. 2(c), G peak and 2D peak lie at 1582 cm^{-1} and 2691 cm^{-1} , respectively. The existence of the D peak at 1350 cm^{-1} suggests the presence of defects during the wet-transfer process.

Figure 3(a) depicts the transmission spectra for the device without graphene (solid line) and with graphene (dash line). The ER of the transmission spectrum for the device without the graphene is $\sim 25 \text{ dB}$. After transferring the graphene sheet onto the PCN cavity, the bandwidth increases and the ER decreases to 8 dB due to the absorption of the graphene

sheet. The transmission spectra of the device at different heating powers are provided in Fig. 3(b). When the heating power is 1.76 mW with a bias voltage of 8 V, the resonance wavelength shows a red shift of 2.64 nm. Figure 3(c) describes the resonance wavelength shift as a function of the heating power, and the TO tuning efficiency (η) is calculated to be 1.5 nm/mW. In the experiment, grating couplers were used to couple light into and out of the chip with single mode fibers. For the device without graphene, the input and output powers are 6 dBm and -7 dBm, respectively. The total loss of the device is 13 dB, including the coupling loss of the grating couplers (~ 13 dB) and negligible insertion loss of the PCN cavity. After transferring the graphene, the insertion loss of the device increases to 2 dB due to the graphene absorption. The total resistance of our device is calculated by $R = U/I$, where R , U and I are the total resistance of the device, the bias voltage and the output current, respectively. According to the equation, we calculated the total resistance $R = 8 \text{ V}/0.22 \text{ mA} = 36 \text{ k}\Omega$, including the resistance of the two Au electrode/graphene contacts ($R_1 + R_3 = 4 \text{ k}\Omega$) and the resistance of the graphene micro-heater ($R_2 = 32 \text{ k}\Omega$). In the device, the resistance of the graphene micro-heater can be calculated as $R_2 = R_s \times L_g/W_g = 2.78 \text{ k}\Omega$ where $R_s = 1 \text{ k}\Omega/\text{sq}$ is the sheet resistance of the graphene sample, $L_g = 5 \text{ }\mu\text{m}$ and $W_g = 1.8 \text{ }\mu\text{m}$ are the length and the width of the graphene, respectively. Note that the measured resistance of the graphene micro-heater ($\sim 32 \text{ k}\Omega$) is higher than that of the theoretical calculation ($\sim 2.78 \text{ k}\Omega$). It can be attributed to cracks and wrinkles of the graphene sheet, which were observed by an optical microscope if the graphene sheet was transferred onto a SiO_2 (285 nm) wafer through the same transfer process. By improving the wet-transfer process of the graphene, the graphene sheet quality can be optimized. The contact resistance ($\sim 4 \text{ k}\Omega$) is also higher than that in [19–21] which might be attributed to the poor wettability between Au electrodes and the graphene [22]. One can reduce the contact resistance by using a lower wettability metal (Pd) as the metal electrode, thus concentrating more heat power into the PCN cavity subsequently leading to a higher TO tuning efficiency.

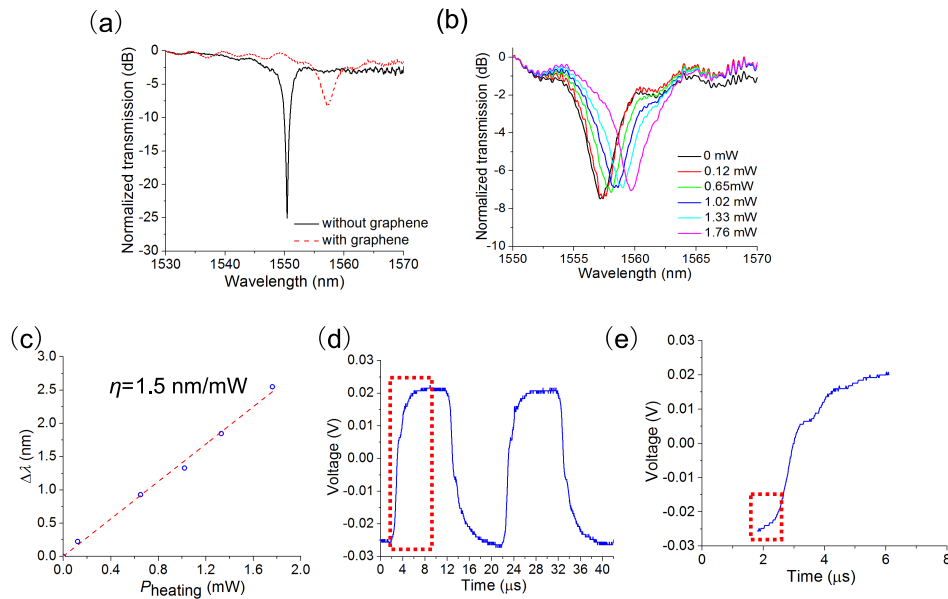


Fig. 3. (a) Normalized transmission spectra of the device with a gap of 70 nm. (b) Normalized transmission spectra at different heating powers. (c) Fitting curve of the resonance wavelength shift $\Delta\lambda$ as a function of the applied heating power P_{heating} . η : TO tuning efficiency. (d) Dynamic response of the heater measured by detecting the transmitted light. (e) Zoom-in view of the output signal. The distorted region is shown by the red dashed lines.

The response time of the PCN cavity is also evaluated, which is an important parameter for TO tuning devices. A square-waveform electrical signal is applied to the graphene micro-heater with a probe wavelength fixed at 1557.55 nm. The peak-to-peak voltage and the frequency of the driving signal are set to 3 V and 50 kHz, respectively. The modulated light is detected by an optical receiver whose electrical output is sent to an oscilloscope. Owing to the relatively flat notch of the transmission spectra of the PCN cavity [see Fig. 3(b)], the output signal is distorted under the low bias voltage as shown in Figs. 3(d) and 3(e). Although the distorted region is a small part of the temporal response signal, the 10%-90% rule is not suitable for our device to extract the intrinsic alternating current (AC) properties of the graphene/waveguide heating process [21]. Instead, time constants are used while the distorted region is excluded in the fitting process to obtain accurate time constants. Thus the time constants are estimated to be $\tau_{\text{rise}} = 1.11 \mu\text{s}$ and $\tau_{\text{fall}} = 1.47 \mu\text{s}$ by fitting the rise and fall edges of the waveform with exponential decay functions of $1 - \exp(-t/\tau_{\text{rise}})$ and $\exp(-t/\tau_{\text{fall}})$ [23], which are much faster than those of metal heaters [24]. Such fast response times originate from the excellent thermal conductivity of the graphene.

4. Discussion

In order to clarify the influence of the graphene on the transmission spectra of the device, the cross-section electric-field distribution in the PCN cavity at the black dashed-line position in Fig. 1(a) is simulated by using the commercial software COMSOL. In the simulation, the refractive index and the thickness of PMMA are set to 1.49 and 200 nm, respectively. As depicted in Fig. 4(a), the real and imaginary parts of the effective modal index (n_{eff}) are 2.411 and 0.003059 for the $500 \times 220 \text{ nm}^2$ single-mode silicon waveguide with the PMMA-covered graphene, respectively. The field distribution of the waveguide without the graphene is also investigated [see Fig. 4(b)] where n_{eff} is equal to 2.39. One can find that the real and the imaginary parts of n_{eff} both increase by introducing PMMA-covered graphene. Since the resonance wavelength is determined by the real part of n_{eff} , the resonance shift can thus be observed in the experiment [25]. Moreover, the quality factor and the ER of the PCN cavity both decrease due to the increased loss in the cavity which is determined by the imaginary part of n_{eff} [25]. Note that, the reduced quality factor and ER can be improved by reducing the loss in the cavity through using the p-doped graphene [26] or tuning the Fermi level of the graphene [13].

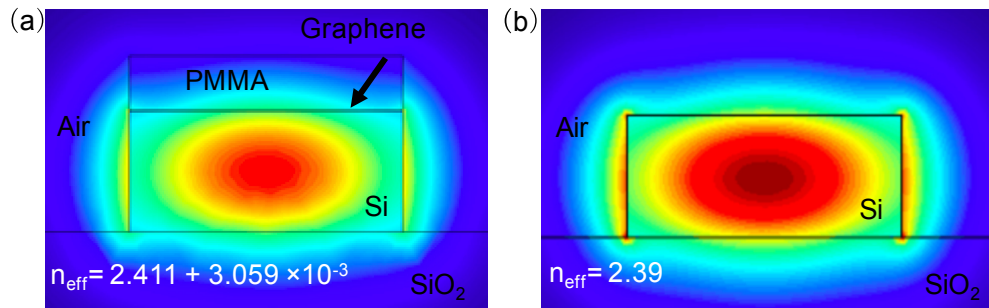


Fig. 4. (a) Electric-field distribution of TE mode of the PCN cavity with PMMA-covered graphene corresponding to the black dashed-line position in Fig. 1(a). (b) Electric-field distribution of TE mode of the PCN cavity without graphene.

To analyze and further increase the TO tuning efficiency of the fabricated device, 3D finite element method (FEM) simulations are performed to study the temperature distribution of the device in the heating process. In the simulations, the thermal conductivities of the graphene, the silicon, and the silica are set to $\sim 2,000 \text{ W/m} \cdot \text{K}$, $\sim 80 \text{ W/m} \cdot \text{K}$, and $\sim 1.38 \text{ W/m} \cdot \text{K}$, respectively [20]. The heat convection coefficient of air is set to $\sim 5 \text{ W/m}^2 \cdot \text{K}$. And the thickness of the graphene is chosen as 0.5 nm. Figure 5(a) depicts the temperature distribution

in the silicon nanobeam cavity when the heating power is 2 mW. The thermal distribution of xy cross section of the device is shown in Fig. 5(b). The temperature of the silicon in the PCN cavity increases from 300 K to 360 K. Note that, the length of the graphene micro-heater ($L_g = 5 \mu\text{m}$) is much longer than the width of the nanobeam waveguide ($w = 0.5 \mu\text{m}$) and part of the heating energy is lost in the electrical connections as shown in Fig. 5(a). Thus the TO tuning efficiency can be increased if the length of the electrical connections, denoted as L_{c1} and L_{c2} , are decreased. One can shorten them after filling the gap and trenches [see Fig. 1(d)] with SiO_2 and polishing the device with chemical mechanical polishing (CMP) process [14]. Based on the analysis, an optimized structure is proposed in Fig. 5(c). As the minimum distance between the metal electrode and the waveguide is $0.5 \mu\text{m}$ to minimize the optical absorption effect [13], L_{c1} and L_{c2} are set to $0.5 \mu\text{m}$ and $1 \mu\text{m}$, respectively. Then the length of the graphene micro-heater decreases from $5 \mu\text{m}$ to $2 \mu\text{m}$. Simulations are performed to study the thermal distribution of xy cross section of the optimized structure. When the heating power is 2 mW, the temperature of the silicon in the PCN cavity increases from 300 K to 452 K as shown in Fig. 5(d). The TO tuning efficiency can be expressed as $\eta = \Delta\lambda/P = \Delta\lambda/\Delta T \times \Delta T/P$, where $\Delta\lambda$, P , and ΔT are the resonance wavelength shift, the heating power and the temperature variation in the PCN cavity, respectively. In the fabricated device and the optimized structure, the parameters for the PCN cavities are the same and thus $\Delta\lambda/\Delta T$ keeps almost unchanged. Note that, $\Delta T/P$ in the optimized structure is 2.5 times higher than that in the fabricated device based on the FEM simulation results. Then the tuning efficiency η , proportional to $\Delta T/P$, is expected to increase to 3.75 nm/mW for the optimized structure. Moreover, the TO tuning efficiency can also be significantly increased by using free-standing structures [7, 27].

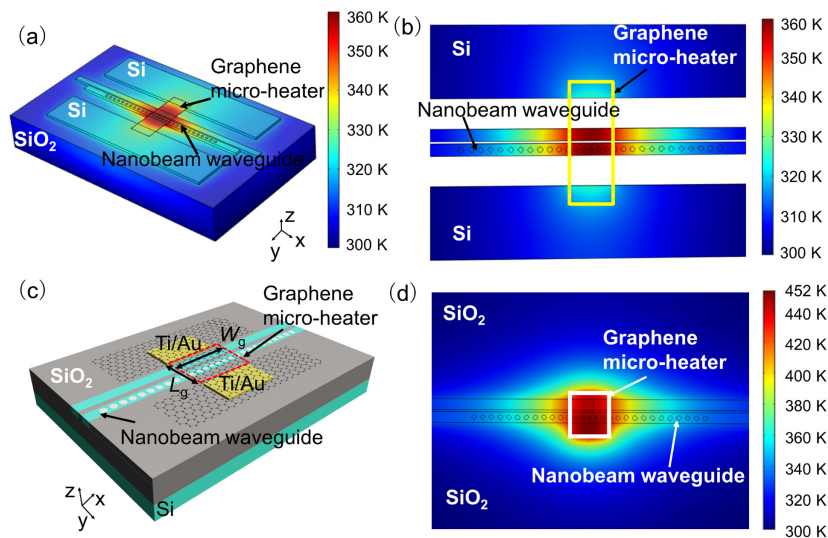


Fig. 5. (a) Three-dimensional temperature distribution of the device in the experiment. (b) Corresponding thermal distribution of xy cross section of the device in (a). The graphene micro-heater is shown by the yellow solid lines. (c) Three-dimensional schematic illustration of the optimized structure. The length of the graphene micro-heater is reduced to $2 \mu\text{m}$. (d) Thermal distribution of xy cross section of this optimized device in (c). The graphene micro-heater is shown by the white solid lines.

5. Summary

In summary, an ultra-compact tunable silicon PCN cavity with an energy-efficient graphene micro-heater is proposed and experimentally demonstrated. Owing to the ultra-compact device footprint and strong confinement of light within a small mode volume of the PCN

cavity, the light-matter interaction is highly enhanced. In the experiment, the TO tuning efficiency is measured to be 1.5 nm/mW. The time constants with a rise time constant of $\tau_{\text{rise}} = 1.11 \mu\text{s}$ and a fall time constant of $\tau_{\text{fall}} = 1.47 \mu\text{s}$ are obtained. Furthermore, the TO tuning efficiency can be increased to 3.75 nm/mW in an optimized structure by reducing the length of the electrical connections of the graphene micro-heater. The proposed device has a high TO tuning efficiency and a fast response time, which could be a functional component for reconfigurable photonic networks.

Funding

This research was supported in part by the National Natural Science Foundation of China (NSFC) under Grant No. 61505104/61235007/61605112, in part by the National Key R&D Program of China No. 2016YFB0402501, and in part by the Science and Technology Commission of Shanghai Municipality under Grant No. 15ZR1422800/16XD1401400.

Acknowledgments

We acknowledge the support of device fabrication by the Center for Advanced Electronic Materials and Devices of Shanghai Jiao Tong University.